Hindawi
BioMed Research International
Volume 2023, Article ID 8836756, 11 pages
https://doi.org/10.1155/2023/8836756

Research Article

Characterization and Analysis of HEK293/Adenovirus Type 5 Cell Cultures under Simulated Microgravity Using Differential Neural Network Modeling

Carlos A. Tavira-Montalvan,[1] **Alejandro Garcia-Gonzalez**,[2] **and Angélica Meneses-Acosta**[1]

[1]*Laboratorio 7 de Biotecnología Farmacéutica, Facultad de Farmacia, Universidad Autónoma del Estado de Morelos, Av. Universidad 1001, Col Chamilpa, Cuernavaca, Morelos, C.P. 62209, Mexico*
[2]*Tecnologico de Monterrey, Escuela de Medicina y Ciencias de la Salud, Av. General Ramon Corona 2514, Nuevo México, Zapopan, Jalisco, Mexico C.P. 45138*

Correspondence should be addressed to Angélica Meneses-Acosta; angelica_meneses@uaem.mx

Received 23 December 2022; Revised 17 July 2023; Accepted 24 July 2023; Published 14 August 2023

Academic Editor: Syed Hassan

HEK293 cells are the common system to produce adenoviral vectors for vectorized vaccines and gene therapy products. Therefore, the improvement of this type of cell culture is highly relevant nowadays. Furthermore, the high aspect ratio vessel (HARV) bioreactor provides a simulated microgravity condition (SMGC) which allows the establishment of *in vitro* models of mammalian cells. The present work is aimed at showing the characterization of HEK293 cell cultures in serum-free medium under SMGC and to identify a set of adaptable time differential equations from experimental data through a nonparametric mathematical modeling using differential neural networks (DNN). Results showed that the HARV bioreactor enables to obtain a gravity percentage equal to ⟦%g⟧_maximum = −0.053% (where minus sign implies against the gravity direction). In addition, the characterization of HEK293 culture under SMGC revealed that such condition favored the production of infective viral particles as well as the uptake of basic nutrients such as glucose and glutamine, but the cell concentration was not significantly affected. As shown, these results contribute to improve the adenoviral vector production, and the DNN analysis is useful to model the kinetic changes and to build the foundations for control strategies and optimization of adenoviral production in further studies.

1. Introduction

Human embryonic kidney 293 (HEK293) cells are the common system for adenovirus production. This type of cells has been used since 1977 [1] due to the fact that they were cloned with the E1 region of Ad5, so they allow the propagation of nonreplicative adenoviruses and other types of viral vectors [2]. These cells originally were grown as adherent cells, but nowadays, there are different clones that grow in suspension cultures, and their use has been increased for the production of biopharmaceuticals and gene therapy vectors [3]. In addition, adenoviral vectors as gene delivery systems have interesting characteristics such as relative easy manipulation, high production titers (up to 10^{12} VP/mL), high tropism of infection, episomal genome into the host cell, and high immunogenicity [4]. Currently, the HEK293/adenovirus system is a key element in the production novel vaccines against various infectious agents such as SARS-CoV-2 [5–7].

In another hand, during the early 1980s, the National Aeronautics and Space Administration (NASA) started to develop bioprocesses using mammalian cell culture in space and studying the microgravity environment (10^{-2} to 10^{-6} g). Some advantages demonstrated by such environment were that the absence of gravity-driven convection reduced the hydrodynamic shear stress and decrease of hydrostatic pressure as well as a significant decrease on cell sedimentation [8,

9]. To create microgravity conditions, NASA developed the patented rotating wall vessel (RWV) bioreactor by Synthecon Inc., which is a rotary cell culture system (RCCS) that simulates microgravity. The high aspect ratio vessel (HARV) is one of the RCCS designs. HARV is a device that allows establishing an experimental setup where there is not a consistent gravitational field. HARV design allows the establishment of *in vitro* models of mammalian cells. Furthermore, it can be applied in the implementation of organotypic cultures, host-pathogen interaction models, evaluation of new therapeutic targets, toxicology, and evaluation of new drugs [10–12]. Microgravity devices have allowed the establishment of cultures for cell therapy protocols focused on optimizing stem cell cultures [13] and understanding and identifying therapeutic targets for diseases such as cancer [14] and the generation of three-dimensional cultures on the development of new drugs in tissue engineering [15].

In addition, mathematical modeling and validation of coupled cell motion, nutrient transport, and cell culture kinetics are still a challenge for rotating and nonrotating bioreactors used for mammalian cell culture [16]. In this regard, the dynamic system identification approach is a reliable alternative to build a mathematical model from observed input-output datasets [17]. System identification theory deals with the problem of extracting governing equations from experimental data because it considers that data are abundant whereas models often remain elusive [18]. The identification procedure is characterized by three main components: the dataset, the set of candidate models, and the estimation method [19]. Particularly, differential neural networks (DNN) have been successfully implemented for nonparametric identification of highly nonlinear bioprocess. In this context, this work presents the effect of SMGC on the production of adenoviral vectors using HEK293 cells, as well as the implementation of DNN for the nonparametric identification of this process and an input-output modeling created by this set of adaptive differential equations, which model the kinetic changes and allow to propose new control strategies to optimize the adenoviral vector production in further studies. So, the characterization described in this work is of great importance in order to improve the knowledge of biopharmaceutical-producing cultures.

2. Methodology

2.1. HEK293 Cells. Human embryonic kidney cell line (HEK293) was obtained from the ATCC (ATCC catalog no. CRL-1573). Initially, HEK293 cells were cultured in DMEM F12 (Gibco, catalog no. 12500062) and 10% FBS (ByProducts Batch No. FBS19003, catalog no. 90020), and then, such cells were adapted to Excell 293 serum-free medium (Sigma, catalog no. 14571C) and supplemented with 4 mM of glutamine (Sigma, catalog no. G8540). Cells were incubated at 37°C, 5% CO_2, and 95% humidity in an Eppendorf® New Brunswick™ S41i incubator.

2.2. Type 5 Adenoviral Vector/Gamma Interferon (Ad5/γ-inf) Stock. Nonreplicative adenoviral vector type 5 that expresses gamma interferon (*Ad5/γ-inf*) was generated in the Laboratory 7 of Faculty of Pharmacy at the Autonomous University of the State of Morelos, Mexico [20]. Briefly, the Adeno-X™ Expression System1 kit (Clontech cat. no. PT3414-1) was used for the molecular construction of *Ad5/γ-inf* gamma. Amplification was done by 6 consecutive passages reaching a viral titer stock of 3.6×10^{11} PFU/mL. The viral titer was determined by the endpoint dilution method [21].

2.3. The Rotary Cell Culture System- (RCCS-) HARV. The microgravity condition was simulated in a rotating cell culture system (RCCS-1), type high aspect ratio autoclavable vessel (HARV) (Houston, Texas 77054, USA). Such a device has a diameter of 99.06 mm, a depth of 6.33 mm, and a total volume of 50 mL. The extra volume of culture medium (approximately 10 mL) was used to remove air from the system which is removed with the syringes from the filling ports. The rotation speed for HEK293 cell cultures was finally determined as 25 rpm (as shown in the results). Operation of the HARV system was done inside of an incubator (Thermo Fisher Model Series 3 water jacketed) at 37°C, 5% CO_2, and 95% humidity in a BSL2 laboratory.

2.4. Assessment of Microgravity Conditions in the Experimental Setup. Microgravity conditions during the experiments were evaluated by an image processing approach. Trajectories of HEK293 cell spheroids inside the bioreactor were recorded to estimate the resultant gravity component during rotation. An embedded CCD video camera (POXXXJS2-3, 13 megapixels) of a cellular phone (Huawei P smart) was implemented to register the spheroid's trajectories. The camera and the bioreactor were positioned inside the biosafety cabinet, 30 cm apart and perpendicular to the image plane. Experiments were recorded, and videos were saved in mp4 format to be processed offline. The schematic representation of trajectories is shown in Figure 1. Later, videos were decomposed into frames (jpg format), according to the camera's time resolution to an interval of one-third of a second (1/3 s) between them. A 9.96 cm radius was chosen in order to establish the pixel/cm ratio. Open-source software Kinovea 0.8.15 and ImageJ 1.53 were used to perform this process. In each frame, the trajectory of this point through each cycle was registered with a pair of coordinates on the image labeled as $C_i(x(n), y(n))$, where C_i corresponds to the geometric center of the ith spheroid and $x(n), y(n)$ correspond to the coordinates on each nth frame in meters. The coordinates of a complete trajectory during one revolution were used to determine the average linear velocity $v(n)$ and acceleration $a(n)$ at each frame. These variables are given by the following functions depending on x coordinates and on time, where $t(n)$ and $t(n-1)$ correspond to the time registered during the n and the previous $(n-1)$ frame: $v_x = x(n) - x(n-1)/t(n) - t(n-1)$, and $a_x = v_x(n) - v_x(n-1)/t(n) - t(n-1)$. Analogous expressions were used for the determination of components $v_y(n)$ and $a_y(n)$. The magnitude and direction of $v(n)$ and $a(n)$ were calculated and depicted in their vectorial representation over the image plane. To estimate the fraction of gravity acceleration over each spheroid at each n frame, the following calculation was performed: gravity fraction $(n) = (a_Y(n) * 100)/-g$, where $g = 9.81\ \mathrm{m/s^2}$.

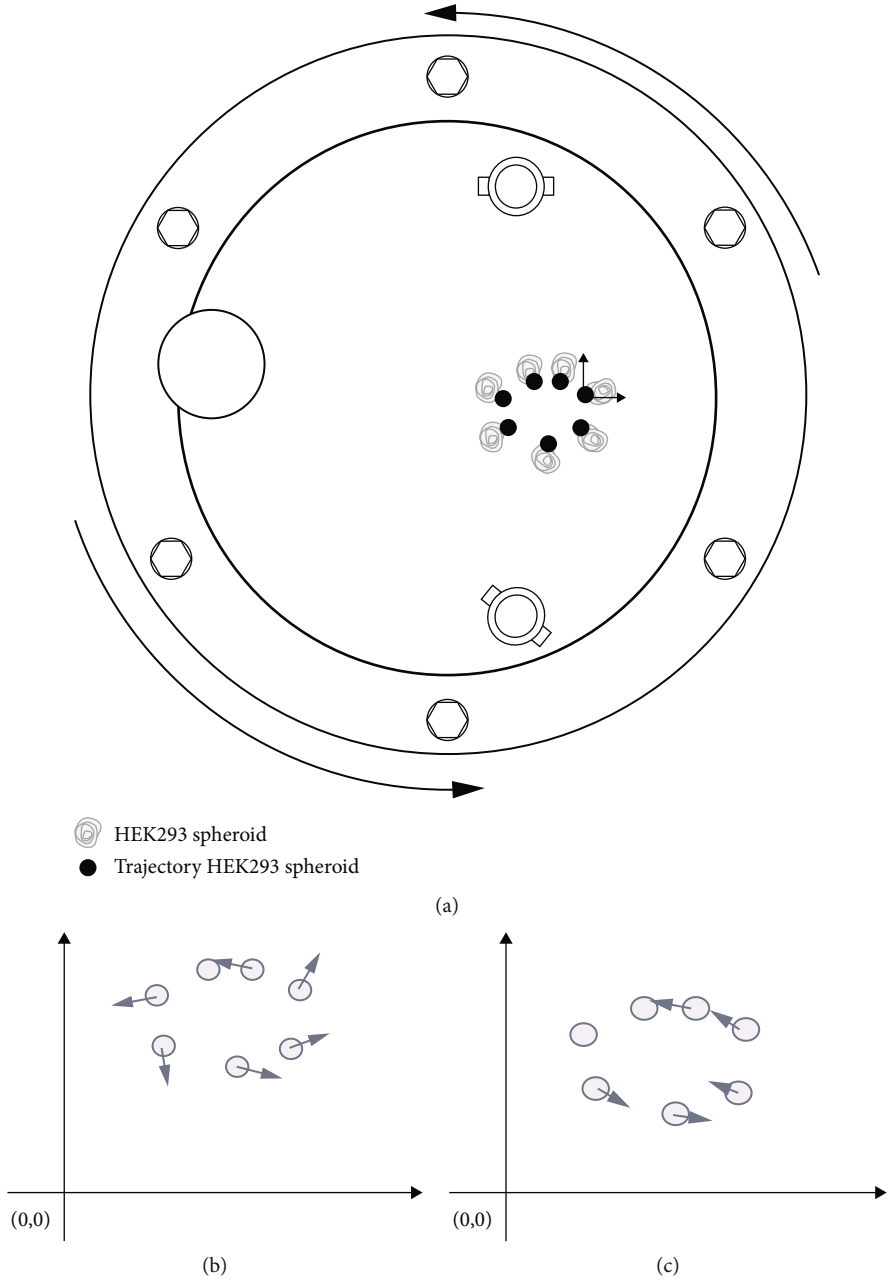

Figure 1: Determination of HEK293 cell gravity percentage under SMGC. (a) Trajectory plot of HEK293 cells taken from digital processing of photograms at an agitation speed of 25 rpm. (b) Representation of velocity vector of the HEK293 cell spheroid. The calculated average value for velocity vector magnitude was $\lfloor v \rfloor = \sqrt{v_x^2 + v_y^2} = 0.016$ m/s S.D. 0.0026 m/s. (c) Representation of acceleration vector of the HEK293 cell spheroid. The calculated average value for the acceleration vector magnitude was $\lfloor a \rfloor = \sqrt{a_x^2 + a_y^2} = 0.0366\ \text{m/s}^2$ S.D. $0.0204\ \text{m/s}^2$. Considering acceleration on y-axis, minimum and maximum values were $a_{y\,\text{minimum}} = -0.015\ \text{m/s}^2$ and $a_{y\,\text{maximum}} = 0.0052\ \text{m/s}^2$ (minus sign indicates downward direction); the percentage of gravity of this minimum and maximum vertical acceleration perceived by the HEK293 cells in the HARV culture system were $\%g_{\text{minimum}} = 0.153\%$ (downward direction) and $\%g_{\text{maximum}} = -0.053\%$ (where minus sign implies against the gravity direction); this is the fraction of gravity considering $g = 9.81\ \text{m/s}^2$. The effect of gravity is minimum in the downward direction, compensated for the rotational system.

2.5. HEK293 Cell Culture Characterization under Simulated Microgravity Conditions (HARV: SMGC) and under Earth's Gravity Conditions (Shake Flask Cultures: EGC). HEK293 cell culture growth kinetics were established in SMGC using 50 mL of Excell 293 serum-free medium with an inoculum of 2×10^5 cells/mL and maintained at 37°C and 5% CO_2; HARV rotation speed was 25 rpm in all the experiments. These cell cultures were compared to the ones of HEK293 in EGC using 250 mL shaken flasks (using 50 mL of culture medium) at 100 rpm into an orbital shaker incubator

(Eppendorf® New Brunswick™ S41i) with a volume of 50 mL of Excell 293 serum-free medium with an initial inoculum of 2×10^5 cells/mL at 37°C and 5% CO_2.

2.5.1. Cell Counting and Viability. The amount of total and viable cells per mL was determined by the trypan blue (Gibco, catalog no. 15250061) exclusion technique [22].

2.5.2. Nutrient Measurement. Glucose, glutamine, lactate, and glutamate were measured on a YSI biochemical analyzer (YSI model 2900).

2.6. Ad5/γ-inf Infection Kinetics. HEK293 cell cultures at SMGC and EGC were infected by the recombinant vector *Ad5/γ-inf* using a multiplicity of infection (MOI) of 5 and a cell density of 0.6×10^6 cell/mL; such conditions were previously established by Sosa-García [23]. γ-Interferon (γ-inf) expression and adenovirus titers were sampled at 72 h, 96 h, and 120 h. Supernatants were stored at -20°C and dry pellets at -80°C for subsequent analysis using protease inhibitor. γ-inf expression was measured by the ELISA platinum kit (Invitrogen BMS228). Adenovirus titer was determined by the Reed and Muench method [21].

2.7. Nonparametric Dynamic Identification by Differential Neural Networks

2.7.1. Identification Assumptions and Experimental Dataset. For the nonparametric identification of the process, the cell culture system in a batch operating condition (no input flow) was represented by the general class of continuous nonlinear systems, set out by the following set of ordinary differential equations:

$$\frac{dx(t)}{dt} = f(x(t)) + \xi(t), \tag{1}$$

where $x(t) \in R^n$ is the state vector at time $t \geq t_0$, with a given initial condition $x(t_0)$. In the particular case of kinetic of growth, $x(t) \in R^5$ for noninfected experiments, and $x(t) \in R^7$ for the infected experiment, with the following components: $x_1(t)$ is the cell concentration (cell/mL), $x_2(t)$ is the viral production (PFU/mL), and $x_3(t)$ is the interferon production, at current time t. The $\xi(t) \in R^n$ is an additive bounded vector of deterministic noise affecting the state vector which considers the possible experimental noise. Experimental values of each variable in state vector $x(t) \in R^n$ were registered offline and preprocessed by simple fitting polynomial regression to build a continuous time-series dataset. This dataset is used to estimate the dynamic model given by adaptive differential equations as it is described below.

2.7.2. Differential Neural Network Modeling Structure. The following approach was based on the methodology presented in Gradilla-Hernández et al. [24]. A differential neural network (DNN) is an adaptive nonlinear differential equation used to approximate the right-hand side $f(x(t))$ of the system (1); such approximation depends on the time-varying parameters (weights, $W(t)$) which must be adjusted by a concrete learning law. This set of differential equations involves two parts: a linear section represented by a Hurwitz matrix $A \in R^{nxn}$ with constant components and an adaptable nonlinear section with time-variable sigmoid functions multipliers $\sigma(x(t))$ (vector of activation functions); this is

$$\frac{d\hat{x}(t)}{dt} = A\hat{x}(t) + W(t)\sigma(\hat{x}(t)), \tag{2}$$

where $\hat{x} \in R^n$ is the estimated state vector by the DNN, $A \in R^{nxn}$, $W \in R^{nxp}$, and $\sigma(\cdot) \in R^{px1}$. The constant parameters as well as the time-varying parameters should be properly adjusted to guarantee a correct state approximation between $x(t)$ and $\hat{x}(t)$. Matrix $W(t)$ provides the adaptive capacity of the DNN and is given by the solution of the following set of differential equations:

$$\begin{aligned} &\frac{dW(t)}{dt} = -(2k)^{-1} P\Omega\left(\hat{x}(t), \hat{x}(t-h(t))\sigma^{\top}(\hat{x}(t)\right) + (2k)^{-1} P\hat{W}(t), \\ &\Omega\left(\hat{x}(t), \hat{x}(t-h(t))\right) = 2\delta(t-h(t)) + \hat{W}(t)\sigma(\hat{x}(t)), \end{aligned} \tag{3}$$

where $\delta := \hat{x}(t) - x(t)$ is the identification error, $\hat{W}(t) = W(t) - \hat{W}$ for a given $\hat{W}$, $k > 0$ is the adaptation rate, and P is a matrix with the following characteristics: $P \in R^{nxn}$, $P = P^{\top}$.

The set of parameters for the DNN identifier for noninfected experiments ($x(t) \in R^5$) is selected as linear stable matrix $A = -0.03 \times I^{5\times5}$, the adaptable weight matrix as a diagonal array $W_1(t) = [w_{11}(t)\,0\,0\,0\,0; 0\,w_{22}(t)\,0\,0\,0; 0\,0\,w_{33}(t)\,0\,0; 0\,0\,0\,w_{44}(t)\,0; 0\,0\,0\,0\,w_{55}(t)]$, and the vector of sigmoid functions $\sigma(\hat{x}(t)) = [\sigma_1(\hat{x}_1(t))\,\sigma_2(\hat{x}_2(t))\,\sigma_3(\hat{x}_3(t))\,\sigma_4(\hat{x}_4(t)), \sigma_4(\hat{x}_4(t))]$; then, the particular nonparametric identification structure (dynamic model) is given by

$$\begin{aligned} \begin{bmatrix} \frac{d\hat{x}_1(t)}{dt} \\ \frac{d\hat{x}_2(t)}{dt} \\ \frac{d\hat{x}_3(t)}{dt} \\ \frac{d\hat{x}_4(t)}{dt} \\ \frac{d\hat{x}_5(t)}{dt} \end{bmatrix} &= \begin{bmatrix} -0.03 & 0 & 0 & 0 & 0 \\ 0 & -0.03 & 0 & 0 & 0 \\ 0 & 0 & -0.03 & 0 & 0 \\ 0 & 0 & 0 & -0.03 & 0 \\ 0 & 0 & 0 & 0 & -0.03 \end{bmatrix} \begin{bmatrix} \hat{x}_1(t) \\ \hat{x}_2(t) \\ \hat{x}_3(t) \\ \hat{x}_4(t) \\ \hat{x}_5(t) \end{bmatrix} \\ &+ \begin{bmatrix} w_{11}(t) & 0 & 0 & 0 & 0 \\ 0 & w_{22}(t) & 0 & 0 & 0 \\ 0 & 0 & w_{33}(t) & 0 & 0 \\ 0 & 0 & 0 & w_{44}(t) & 0 \\ 0 & 0 & 0 & 0 & w_{55}(t) \end{bmatrix} \begin{bmatrix} \sigma_1(\hat{x}_1(t))) \\ \sigma_2(\hat{x}_2(t))) \\ \sigma_3(\hat{x}_3(t))) \\ \sigma_4(\hat{x}_4(t))) \\ \sigma_5(\hat{x}_5(t))) \end{bmatrix}. \end{aligned} \tag{4}$$

This structure is also extended for the infected experiments case to proper dimensions ($x(t) \in R^7$). The given

model after the adjustment of (4) is a set of ordinary differential equation representing the rate of change for every variable considered in the process. It is important to remark that this approach is not a static regression analysis over the time, but a dynamic and adaptable model at any t.

2.8. Statistics. Experiments were performed by triplicate ($n = 3$), and the mean was calculated. Percentage gravity was calculated from frames of three independent experiments (3 cultures in the HARV bioreactor). The error bars represent the standard deviation for each condition. Each variable is approximated by simple polynomial regression to create a continuous time series of data, and a correlation coefficient criterion of greater than 0.95 was set. The structure of the polynomial function is not considered in the analysis and is used exclusively as a continuous data generator.

3. Results and Discussion

3.1. Assessment of the Microgravity Experimental Condition. The processing of obtained images from the recording of the spheroid trajectory of HEK293 cells in DMEM F12 10% SFB medium at 25 rpm allowed the calculation of velocity vector parameters, the acceleration vector, and the gravity fraction for 7 frames that make up the spheroid trajectory in the HARV system. In Figure 1, it is observed that the spheroid trajectory tends to be circular, a pattern that is repeated during each cycle. The velocity (V) of the calculated spheroid was 0.0160 ± 0.0257 m/s with an acceleration (A) of 0.0366 ± 0.0204 m/s^2. Considering acceleration on y-axis, minimum and maximum values were $a_{y\,\text{minimum}} = -0.015\text{m/s}^2$ and $a_{y\,\text{maximum}} = 0.0052$ m/s^2 (minus sign indicates downward direction), the percentage of gravity of this minimum and maximum vertical acceleration perceived by the HEK293 cells in the HARV culture system were $\%g_{\text{minimum}} = 0.153\%$ (downward direction) and $\%g_{\text{maximum}} = -0.053\%$ (where minus sign implies against the gravity direction), and this is the fraction of gravity considering $g = 9.81$ m/s^2. The effect of gravity is minimum in the downward direction, compensated for the rotational system. The comparison between results obtained from experiments performed in Earth's inherent gravity and the ones performed in "true" microgravity (ISS, manned and unmanned spaceflight) or simulated microgravity (rotating walled vessels, clinostats, and rpm machines) allows to observe the biological response of cells in a microgravity environment. The reported magnitude at which microgravity effects can be observed is in the range of 10^{-2} to 10^{-6} g [8, 9, 25, 26].

3.2. HEK293 Cell Culture Characterization under Simulated Microgravity Conditions (HARV, 25 rpm; SMGC) and under Earth's Gravity Conditions (Shake Flask Cultures, 100 rpm: EGC)

3.2.1. 293HEK Cell Growth. The growth of HEK293 cell cultures in Excell 293 medium without serum under SMGC at 25 rpm and EGC in shaken flasks at 100 rpm was compared and is shown in Figure 2(a), A. Specific growth rate for SMGC was 0.0221 h^{-1} with a doubling time of 31 h, and specific growth rate was 0.0247 h^{-1} with a doubling time of 28 h for the EGC. Cell viability for cultures in SMGC was 86% ± 4%, and for EGC (shaken flask), the viability was 80% ± 2% at 144 h. As shown, it is observed that the microgravity condition does not affect the culture development. The calculated values for doubling time for both conditions are within the reported range of 24 h to 56 h for the HEK293 cell line in Excell 293 serum-free medium in Earth's gravity conditions [27, 28]. Doubling time values between SMGC and EGC do not differ significantly, so it can be asserted that the 25 rpm operating condition of the HARV does not negatively impact the growth and viability of HEK293 cells. As we explained before, the choice of shaking cultures of HEK293 cells in suspension as ground gravity control is due to the fact that these are the standard culture conditions for recombinant protein production [29]. It is not possible to use the same speeds at ground and microgravity conditions due to the fact that such values are not comparable, and they are not either optimal for culture development. Cells grown in shaken flasks need a speed of 100 rpm as optimal condition for culture aeration and mass transfer [30, 31] while cells in the HARV bioreactor need an operating speed of 25 rpm to generate the simulated microgravity condition, which was determined in the present work (highlight) following the criteria established by Nickerson et al. for bacteria and particles [32].

Figure 2(a), B shows the process identification by the DNN, the integration of the structure (4), and the adaptation law (3), which allow to represent the estimated differential equation governing the behavior of the variable $x_1(t) =$ cell concentration (cell/mL). For both experimental conditions, the quadratic identification error (DNN estimation vs. experimental data) was determined over the complete time being less than 5% for both cases. This confirms the adaptation and the capacity of the DNN to accurately model this variable. Equivalent results and quality of approximation were obtained for the complete set of state vector variables in all the experimental conditions. Figure 2(a), C shows the growth productivities (cell/mL*h) for both conditions calculated by the DNN approach (2). Both the SMGC and EGC begin to increase their growth rate at 24 h, maximum growth was observed between 48 and 72 h, and from then on, there is a decrease in such a value. After 120 h, there is an increase in the growth productivity under SMGC with respect to the EGC. As reported previously by Lorenzo et al. [27], cell viability remains above 80% at 144 h, and the doubling time is within what is reported in the literature of HEK293 cell cultures in commercial serum-free media for recombinant protein production processes. It should be noted that there are no reference values for HEK293 cell cultures in microgravity environments, so the values reported for EGC in a serum-free medium were considered as a reference.

Complex processes such as the HARV bioprocess are traditionally modeled based on material balances and kinetic relationships; this approach grows rapidly in assumptions that must be considered to keep the number of parameters involved in the equations in a bounded number. Once the

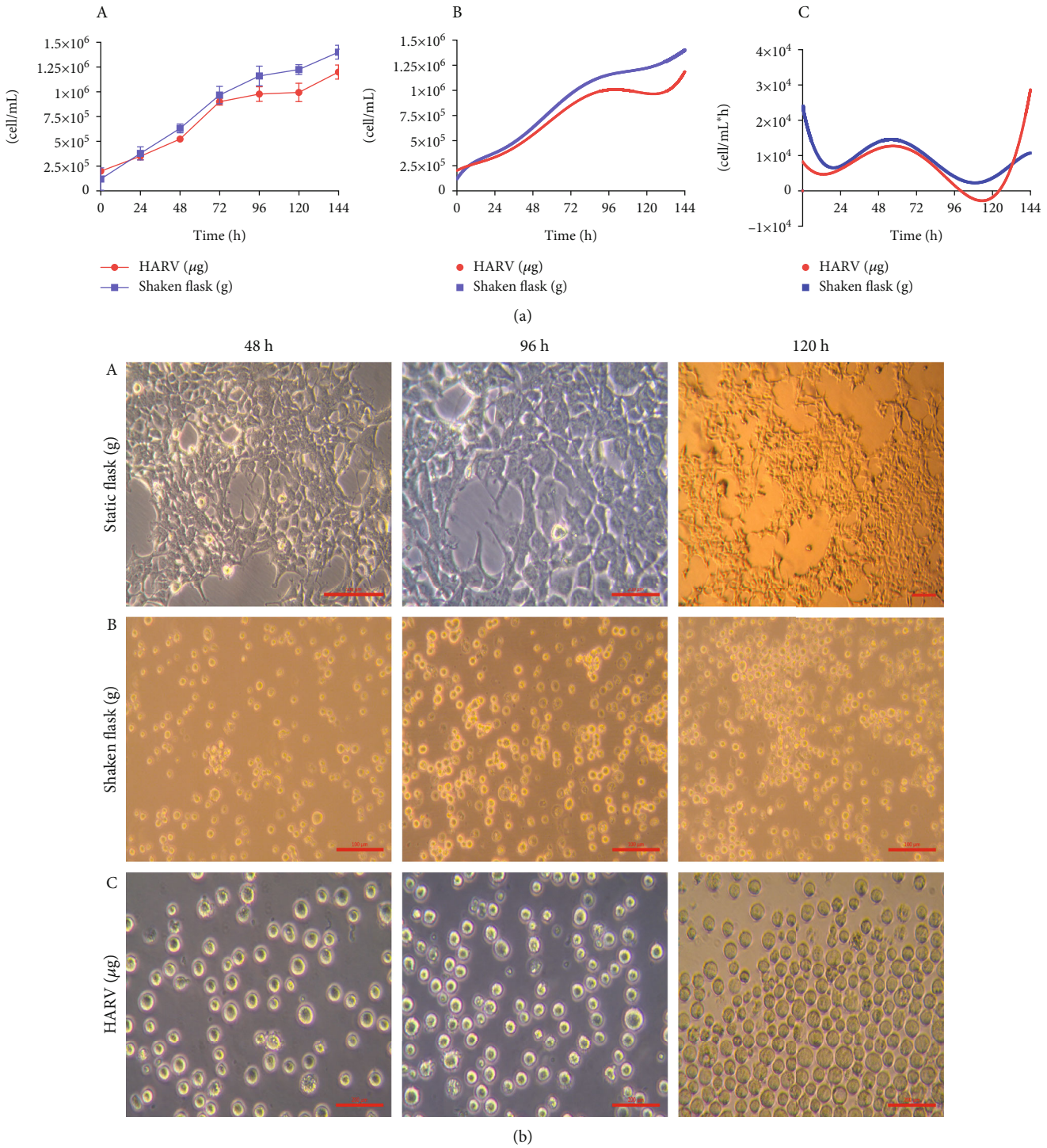

Figure 2: (a) Growth of HEK293 cell culture under SMGC. (A) Growth kinetics of HEK293 cell cultures in the serum-free medium under SMGC and EGC. The doubling time (dt) for μg cultures was 31 h compared to 28 h for EGC in the shake flask. (B) Estimation of HEK293 cell culture growth using a DNN from experimental data. (C) Estimation of cell growth productivities for SMGC and EGC calculated from the DNN approach. Maximum cell growth productivities are observed between 48 and 72 h, after which a decrease in growth rate is observed for both conditions. (b) Morphology of HEK293 cell cultures at 48 h, 96 h, and 144 h 20x. (A) Static HEK293 cell culture in serum-free medium under EGC 20x. Scale bar corresponds to 200 microns (red). (B) HEK293 cell culture in the shake flask in the serum-free medium under EGC. Scale bar corresponds to 100 microns (red). (C) HEK293 cell culture in serum-free medium in HARV bioreactor under SMGC. The scale bar corresponds to 200 microns (red). An evident morphological change is observed. SMGC in the serum HARV bioreactor allows the development of suspension cultures where the cells are spherical without aggregate formation. The EGC in static cultures promotes cell adhesion while in shaken flask cultures the formation of cell aggregates is observed.

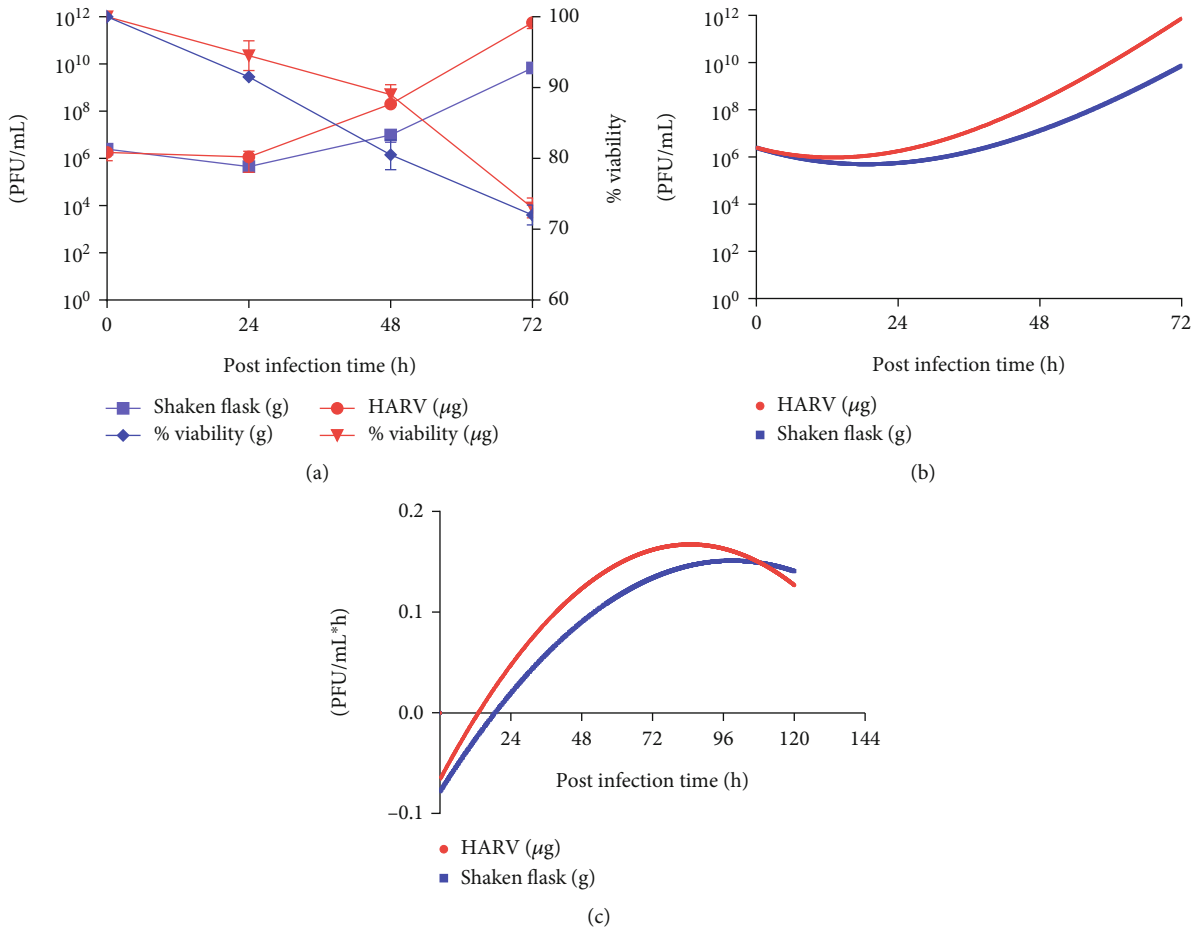

Figure 3: Production of Ad5/g-inf in 293HEK cells under SMGC. (a) Titer of infectious viral particles determined by end-point dilution at 72 h postinfection and % of viability. (b) Estimation of viral titer by a differential neural network (DNN) in HEK293 cell cultures from experimental data. (c). Volumetric production rate of adenoviral particles. As previously reported, the production of adenoviral particles starts after 24 h postinfection in both conditions. The SMGC favored the viral vector production by two exponential values reflecting the value in the volumetric production rate which maximum value was reached at 81.1 h in comparison to the EGC value of 96 h postinfection.

model is derived, each proposed parameter must be calculated, and this implies an extra set of additional experiments to validate them, a situation that in practical conditions is not feasible due to the time consumption and the constant change in real conditions, especially if we pursue the control and optimization of the process; in our case, the microgravity condition is an additional factor to be considered. This situation is avoided through the adaptation strategy of differential neural networks. In this study, an artificial ordinary differential equation system has been implemented as a strategy to model (dynamic identification) the behavior of batch culture of animal cells; with this, we have generated a model that can be used in control applications; this is the first result and the base to propose a future optimization scheme, although this will imply changes in the experimental scheme; setting a control input, it means a fed-batch or continuous operation mode. The modeling strategy based on differential neural networks has proven that it can efficiently approximate the variables involved in the process, thereby becoming an alternative to obtain a representation of a complex process, such as the one implemented, for practical implementations. In this work, we present only the identification (modeling) of the batch system without integrating a control strategy, which would imply a fed-batch scheme or a continuous culture scheme to have a control input. However, once the identification scheme based on differential neural networks is available, there is an artificial structure to propose a controller. An option for this type of process is model-predictive control, where the system model compromises the differential equations of the differential neural network. This strategy allows for predicting the response in a defined time horizon to solve the optimal control based on the system's current state given by the differential neural network model.

The morphological changes of HEK293 cell cultures in Excell 293 serum-free medium cultures at 48 h, 96 h, and 144 h are shown in Figure 2(b). HEK293 cell cultures in serum-free medium in EGC at static culture using T-flasks adhere to the substrate, showing a typical morphology of an anchorage-dependent culture: formation of an extracellular matrix and irregularly and elongated shaped cells [20] (Figure 2(b), A). Suspension cultures in the shake flask under

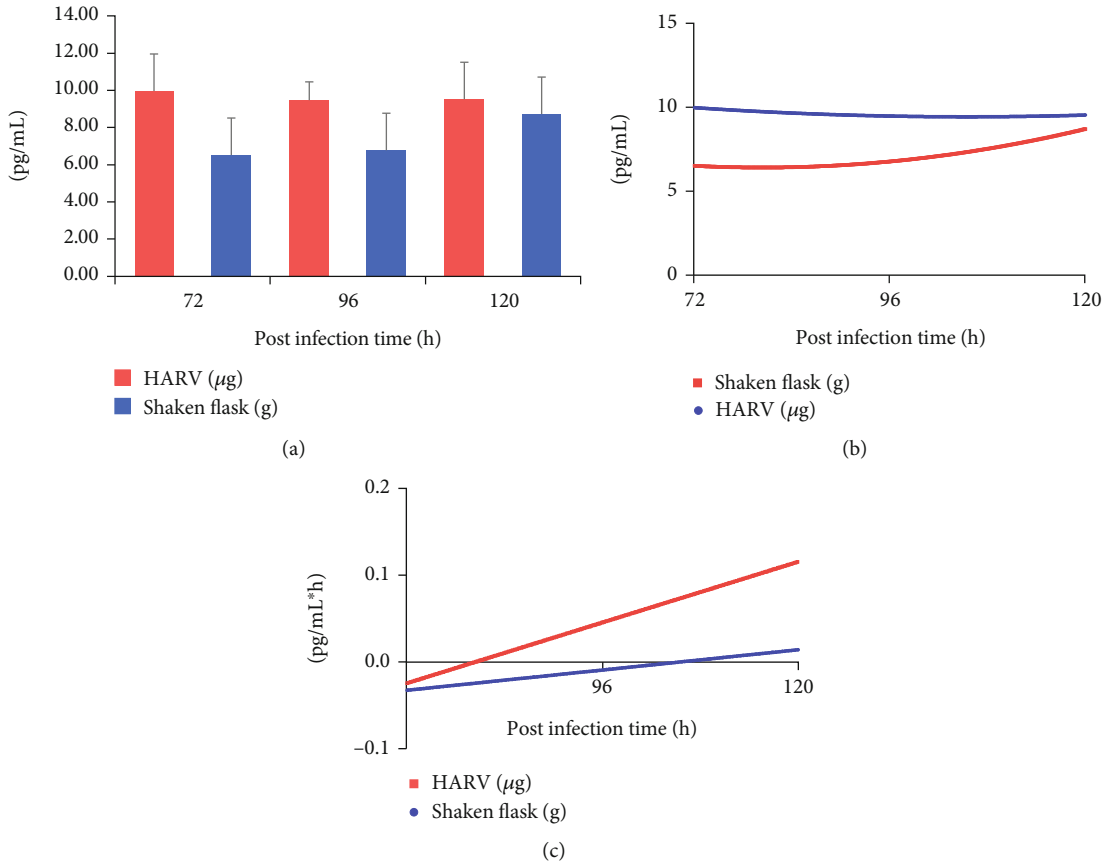

Figure 4: Production of recombinant gamma interferon in 293HEK cells under SMGC. (a) Recombinant gamma interferon concentration determined from supernatants at 72, 96, and 120 h. (b) DNN approach of recombinant gamma interferon concentration with corresponds to the observed experimental data. (c) Gamma interferon volumetric production rates. It is observed that the SMGC predicts a higher volumetric production rate at SMGC (up to 0.11 pg/mL*h for the HARV culture at 120 h postinfection) compared to the EGC values (up to 0.01 pg/mL*h for the shake flask). As observed, no significant difference in concentration was obtained between both conditions, but there is a trend to increase the recombinant protein production in the case SMGC.

EGC are presented in Figure 2(b), B. As observed, the culture tends to form aggregates. This morphology has already been reported in the description of the process of adaptation of anchorage-dependent HEK293 cell cultures to suspension cultures (Figure 2(b), B) [3]. In SMGC, cells present the typical morphology of a homogeneous suspension culture, and no cell aggregates are observed (Figure 2(b), C). This phenomenon is the first time to be reported to our knowledge, and it could be an excellent tool to promote the generation of homogeneous suspension cultures. Until now, one of the main applications of the rotary cell culture system (RCCS) has been the provision of conditions to establish difficult cell cultures such as stem cells, showing that cell viability and morphology are not affected in such conditions [33, 34].

In principle, the phenomenon of mechanotransduction explains the changes in cells in real microgravity and simulated microgravity environments. Cells convert mechanical stimuli into biochemical signals by activating signaling cascades. It has been proposed that gravitational force plays a crucial role in the regulation of cellular and tissue homeostasis by inducing mechanical stresses experienced at the cellular level. It has been reported that the most evident morphological changes of cultured animal cells in SMGC are alterations in cell shape, size, volume, and adhesion properties [35–37]. These morphological changes translate into alterations in transcription, transduction, and organization of the cellular cytoskeleton, mainly associated with microtubules and actin filaments [38].

3.3. Ad5/γ-inf and Gamma Interferon Production. To analyze the production of adenoviral vectors and recombinant protein, HEK293 cell cultures were infected using a multiplicity of infection (MOI) of 5 and a cell density of 0.6×10^6 cells/mL in serum-free medium at SMGC and EGC. As shown in Figure 3(a), viral titer at 72 h postinfection was 9.31×10^{11} PFU/mL and 9.17×10^9 PFU/mL, respectively, which means an increase of 101.5 times for SMGC. As observed, the percentage of cell viability was higher at SMGC than in the case of EGC. The identification by the DNN structure applied to the production of adenoviral particles converges to the experimental data, with an error less than 5% over the identification time. A higher production at the SMGC (Figure 3(b)) is observed. The calculation of volumetric production rates from the DNN network shows that within the first 24 h, the production of adenoviral particles starts at the SMGC, and the culture in the HARV favored the production

Table 1: Specific nutrient consumption rates of glucose and glutamine and specific production rates of lactate and glutamate under SMGC and EGC of HEK293 cell cultures.

Culture condition	qsGlu (pg/cel*h)	qsGln (pg/cel*h)	qpLac (pg/cel*h)	qpE (pg/cel*h)
HARV (SMGC)	666.22 ± 28.20	239.11 ± 14.10	115.08 ± 14.50	23.32 ± 10.70
Shaken flask (EGC)	536.19 ± 14.10	239.08 ± 21.2	142.43 ± 12.20	19.22 ± 8.30
HARV/*Ad5*/*g-inf* (SMGC)	569.79 ± 28.20	4000.00 ± 70.77	817.77 ± 89.80	95.01 ± 21.20
Shaken flask/*Ad5*/*g-inf* (GC)	1111.11 ± 35.30	495.43 ± 56.50	283.34 ± 40.40	39.82 ± 19.50

reaching the maximum value at 84.8 h (0.16 PFU/mL*h), while for the EGC, it is observed at 99 h (0.15 PFU/mL*h). Both conditions begin a deceleration of production later at 96 h (Figure 3(c)). Although specific data on adenovirus production under SMGC are not available, it has been reported that in some cases, microgravity conditions favor the infectivity and capsid assembly of Epstein-Barr virus, human norovirus, hepatitis E virus, and human cytomegalovirus [12, 39]. These observations are consistent with the results presented in this work and support the asseveration that SMGC plus the use of a chemically defined medium promotes a favorable condition to produce infective adenoviral vector particles.

In addition, the identification and quantification of gamma interferon were performed to demonstrate if the recombinant protein production was also affected by the SMGC. Gamma interferon concentrations determined from supernatants at 72, 96, and 120 h are shown in Figure 4(a). The concentration of gamma interferon was 9.53 pg/mL at 120 h for SMGC, while such a value was 8.72 pg/mL for EGC; this shows that there was not a statistically significant difference between both conditions. The low transgene expression is attributed to the fact that the HEK293/Ad5 is mainly directed to the adenoviral vector production. DNN approach with respect to gamma interferon production corresponds to the experimental data. The gamma interferon volumetric production rates maintain a maximum value of 0.11 pg/mL*h) in SMGC and 0.01 pg/mL*h in EGC at 120 h for both cases. There is a higher trend to increase the value in the case of SMGC than in the case of EGC (Figure 4(b)).

3.4. Nutrient Consumption and By-Product Production. Table 1 shows the specific rates of glucose and glutamine consumption, as well as the specific rates of lactate and glutamate production of HEK293 cell cultures in SMGC and EGC, which were calculated in the exponential phase of the cultures. In both SMGC and EGC, there are no drastic differences in the specific rates of glucose (qsGlu) and glutamine (qsGln) consumption. These glucose and glutamine consumption rates agree with other values reported for HEK293 cells in commercial serum-free medium [40]. Lactate and glutamate productions were found to be between previously reported values and without significant differences between the two conditions. However, in the case of cultures infected using the viral vector *Ad5*/*γ-inf*, glucose consumption decreases in SMGC (569.79 ± 28.20 pg/cel*h), and the rate of specific glucose consumption was observed to be 2-fold lower than in the case of EGC (1111.11 ± 35.30 pg/cel*h), causing an enhancement of nutrient uptake by the cells. The specific glutamine consumption is higher in SMGC than in EGC. This result is reflected in the specific rate of glutamine consumption (4000.00 ± 70.77 pg/cel*h), while in EGC cultures, the specific rate of glutamine consumption is 495.43 ± 56.50 pg/cel*h, i.e., about 8 times more. The lactate formation rate (qpLac) shows a difference being lower in EGC with a value of 283.34 ± 40.40 pg/cel*h compared to the lactate formation rate in SMGC of 817.77 ± 89.80 pg/cel*h. This is related to the fact that HEK293 cells present a cometabolisation of glucose and lactate, where lactate is transported to the cytosol and oxidised by mitochondria to generate pyruvate resulting in a more efficient cellular metabolism [41]. This metabolic model does not appear to be affected by SMGC. For glutamate production rates (qpE), a relationship with glutamine consumption is observed 95.01 ± 21.20 pg/cel*h for SMGC and 39.82 ± 19.50 pg/cel*h which explains the difference observed between SMGC and EGC.

4. Conclusion

The percentages of gravity minimum and maximum vertical perceived by the HEK293 cells in the HARV culture system were ⟦%g⟧_minimum = 0.153% (downward direction) and ⟦%g⟧_maximum = −0.053% (where minus sign implies against the gravity direction), and this is the fraction of gravity considering $g = 9.81\ \text{m/s}^2$. The effect of gravity is minimum in the downward direction, compensated for the rotational system. This condition generates benefits in the production of infective adenoviral particles, an order of magnitude above that observed in EGC and a better utilization of the nutrients in the culture medium. The applied differential neural network approach allows to generate a nonparametric model that converges to the dynamic process behavior. This set of adaptive differential equations allows to describe in continuous time the experimental data from the HEK293 cell culture in SMGC versus the data from cultures in EGC. Furthermore, it will allow us to propose a control strategy to optimize the process based on this modeling approach. The results obtained from these experimental sets show that SMGC has broad applications regarding the improvement of mammalian cell culture because it has been shown that this condition helps to get homogenous suspension cultures in an easier and faster way. In addition, the use of SMGC opens up doors to other possibilities such as viral vector production, which, nowadays, is a novel field in cell technology that should be more deeply explored; generation of esferoids as 3D models for nonclinical experimental models to evaluate the effect of different active pharmaceutical compounds; interaction of cells in a 3D models; and model development for cancer studies among other interesting applications.

Data Availability

Data is available on request. Carlos A. Tavira Montalván is authorized to share data information about kinetics and cell calculation. His contact information is carlos.taviramon@uaem.edu.mx. Alejandro Garcia-Gonzalez is authorized to share data information about math modeling. His contact information is alexgargo@tec.mx.

Disclosure

We declare that this manuscript is original, has not been published before, and is not currently being considered for publication elsewhere.

Conflicts of Interest

Carlos A. Tavira-Montalvan, Alejandro Garcia-Gonzalez, and Angélica Meneses-Acosta declare no conflict of interests.

Authors' Contributions

The corresponding author confirms that the manuscript has been read and approved for submission by all the named authors. Carlos A. Tavira-Montalvan developed the experimental work, the analysis and discussion of results, and the writing of this manuscript. Alejandro Garcia-Gonzalez contributed to the DNN establishment and mathematical analysis as well as the financial support for this publication. Angélica Meneses-Acosta contributed the original idea, conceptualization, result discussion, and conclusion as well as the revision of this work.

Acknowledgments

This work was supported by the Consejo Nacional de Ciencia y Tecnología México (CONACyT) and Agencia Espacial Mexicana (SCT, México). Dr. Meneses-Acosta thanks the CONACYT-AEM-2015 Project (262872) for their financial support used in the development of this project. Carlos Tavira thanks the CONACYT's graduate scholarship program (no. 668180). Facilities and equipment were supported by the INFR-2014 Project (226271). We thank Dr. Sergio Alcalá Alcalá and Dr. Jose Antonio Serrato Pérez for their valuable comments.

References

[1] F. L. Graham, J. Smiley, W. C. Russell, and R. Nairn, "Characteristics of a human cell line transformed by DNA from human adenovirus type 5," *Journal of General Virology*, vol. 36, no. 1, pp. 59–72, 1977.

[2] S. Singh, R. Kumar, and B. Agrawal, "Adenoviral vector-based vaccines and gene therapies: current status and future prospects," in *Adenoviruses*, p. 10, IntechOpen, 2019.

[3] M. Malm, R. Saghaleyni, M. Lundqvist et al., "Evolution from adherent to suspension: systems biology of HEK293 cell line development," *Scientific Reports*, vol. 10, no. 1, article 18996, 2020.

[4] J. D. Rubin, T. V. Nguyen, K. L. Allen, K. Ayasoufi, and M. A. Barry, "Comparison of gene delivery to the kidney by adenovirus, adeno-associated virus, and lentiviral vectors after intravenous and direct kidney injections," *Human Gene Therapy*, vol. 30, no. 12, pp. 1559–1571, 2019.

[5] D. Y. Logunov, I. V. Dolzhikova, D. V. Shcheblyakov et al., "Safety and efficacy of an rAd26 and rAd5 vector-based heterologous prime-boost COVID-19 vaccine: an interim analysis of a randomised controlled phase 3 trial in Russia," *The Lancet*, vol. 397, no. 10275, pp. 671–681, 2021.

[6] M. Voysey, S. A. Costa Clemens, S. A. Madhi et al., "Single-dose administration and the influence of the timing of the booster dose on immunogenicity and efficacy of ChAdOx1 nCoV-19 (AZD1222) vaccine: a pooled analysis of four randomised trials," *The Lancet*, vol. 397, no. 10277, pp. 881–891, 2021.

[7] F. C. Zhu, X. H. Guan, Y. H. Li et al., "Immunogenicity and safety of a recombinant adenovirus type-5-vectored COVID-19 vaccine in healthy adults aged 18 years or older: a randomised, double-blind, placebo-controlled, phase 2 trial," *The Lancet*, vol. 396, no. 10249, pp. 479–488, 2020.

[8] C. A. Nickerson, N. R. Pellis, and C. M. Ott, *Effect of Spaceflight and Spaceflight Analogue Culture on Human and Microbial Cells: Novel Insights into Disease Mechanisms*, Springer, 2016.

[9] S. L. Wuest, S. Richard, S. Kopp, D. Grimm, and M. Egli, "Simulated microgravity: critical review on the use of random positioning machines for mammalian cell culture," *BioMed Research International*, vol. 2015, Article ID 971474, 8 pages, 2015.

[10] M. Devarasetty, E. Wang, S. Soker, and A. Skardal, "Mesenchymal stem cells support growth and organization of host-liver colorectal-tumor organoids and possibly resistance to chemotherapy," *Biofabrication*, vol. 9, no. 2, p. 021002, 2017.

[11] M. Moreno-Villanueva, A. H. Feiveson, S. Krieger et al., "Synergistic effects of weightlessness, isoproterenol, and radiation on DNA damage response and cytokine production in immune cells," *International Journal of Molecular Sciences*, vol. 19, no. 11, p. 3689, 2018.

[12] A. L. Radtke and M. M. Herbst-Kralovetz, "Culturing and applications of rotating wall vessel bioreactor derived 3D epithelial cell models," *Journal of Visualized Experiments*, vol. 62, 2012.

[13] X. Lei, Y. Cao, Y. Zhang et al., "Effect of microgravity on proliferation and differentiation of embryonic stem cells in an automated culturing system during the TZ-1 space mission," *Cell Proliferation*, vol. 51, no. 5, article e12466, 2018.

[14] D. Grimm, H. Schulz, M. Krüger et al., "The fight against cancer by microgravity: the multicellular spheroid as a metastasis model," *International Journal of Molecular Sciences*, vol. 23, no. 6, 2022.

[15] Y. Li, L. He, S. Pan et al., "Three-dimensional simulated microgravity culture improves the proliferation and odontogenic differentiation of dental pulp stem cell in PLGA scaffolds implanted in mice," *Molecular Medicine Reports*, vol. 15, no. 2, pp. 873–878, 2017.

[16] D. Selişteanu, D. Endrescu, V. Georgeanu, and M. Roman, "Mammalian cell culture process for monoclonal antibody production: Nonlinear modelling and parameter estimation," *BioMed Research International*, vol. 2015, Article ID 598721, 16 pages, 2015.

[17] L. Ljung, "Perspectives on system identification," *Annual Reviews in Control*, vol. 34, no. 1, pp. 1–12, 2010.

[18] K. Kaheman, J. N. Kutz, and S. L. Brunton, "SINDy-PI: a robust algorithm for parallel implicit sparse identification of nonlinear dynamics," *Proceedings of the Royal Society A*, vol. 476, no. 2242, p. 20200279, 2020.

[19] J. Schoukens and L. Ljung, "Nonlinear system identification: a user-oriented road map," *IEEE Control Systems*, vol. 39, no. 6, pp. 28–99, 2019.

[20] M. N. Romero, *Construcción y evaluación de vectores moleculares que expresen interferón gamma en células humanas como potencial tratamiento inmunoestimulador*, Universidad Autónoma del Estado de Morelos, 2015.

[21] M. A. Ramakrishnan, "Determination of 50% endpoint titer using a simple formula," *Psychological Bulletin*, vol. 6, no. 1, pp. 27-28, 1909.

[22] R. I. Freshney, *Culture of Animal Cells: A Manual of Basic Technique and Specialized Applications*, John Wiley & Sons, 2010.

[23] C. Sosa-García, *Optimización del sistema de expresión HEK293/AD5-IFN-gamma humano mediante el manejo de la densidad celular y la multiplicidad de infección*, Universidad Autónoma del Estado de Morelos, 2018.

[24] M. S. Gradilla-Hernández, A. García-González, A. Gschaedler et al., "Applying differential neural networks to characterize microbial interactions in an ex vivo gastrointestinal gut simulator," *Processes*, vol. 8, p. 593, 2020.

[25] S. Brungs, M. Egli, S. L. Wuest et al., "Facilities for Simulation of Microgravity in the ESA Ground-Based Facility Programme," *Microgravity Science and Technology*, vol. 28, no. 3, pp. 191–203, 2016.

[26] T. C. Chao and D. B. Das, "Numerical simulation of coupled cell motion and nutrient transport in NASA's rotating bioreactor," *Chemical Engineering Journal*, vol. 259, pp. 961–971, 2015.

[27] E. Lorenzo, L. Méndez, E. Rodríguez et al., "Plasticity of the HEK-293 cells, related to the culture media, as platform to produce a subunit vaccine against classical swine fever virus," *AMB Express*, vol. 9, no. 1, p. 139, 2019.

[28] R. Román, M. Farràs, M. Camps et al., "Effect of continuous feeding of CO2 and pH in cell concentration and product titers in hIFNγ producing HEK293 cells: Induced metabolic shift for concomitant consumption of glucose and lactate," *Journal of Biotechnology*, vol. 287, no. October, pp. 68–73, 2018.

[29] C. L. Chin, J. B. Goh, H. Srinivasan et al., "A human expression system based on HEK293 for the stable production of recombinant erythropoietin," *Scientific Reports*, vol. 9, no. 1, 2019.

[30] P. S. Chahal, E. Schulze, R. Tran, J. Montes, and A. A. Kamen, "Production of adeno-associated virus (AAV) serotypes by transient transfection of HEK293 cell suspension cultures for gene delivery," *Journal of Virological Methods*, vol. 196, pp. 163–173, 2014.

[31] D. L'Abbé, L. Bisson, C. Gervais, E. Grazzini, and Y. Durocher, "Transient gene expression in suspension HEK293-EBNA1 cells," *Methods in Molecular Biology*, vol. 1850, pp. 1–16, 2018.

[32] C. A. Nickerson, C. M. Ott, J. W. Wilson et al., "Low-shear modeled microgravity: a global environmental regulatory signal affecting bacterial gene expression, physiology, and pathogenesis," *Journal of Microbiological Methods*, vol. 54, no. 1, pp. 1–11, 2003.

[33] K. D. Kaya, T. DiStefano, L. Gieser et al., "Accelerated and improved differentiation of retinal organoids from pluripotent stem cells in rotating-wall vessel bioreactors," *Stem Cell Reports*, vol. 10, no. 1, pp. 300–313, 2018.

[34] S. Navran, "The application of low shear modeled microgravity to 3-D cell biology and tissue engineering," *Biotechnology Annual Review*, vol. 14, no. 8, pp. 275–296, 2008.

[35] C. Buken, J. Sahana, T. J. Corydon et al., "Morphological and molecular changes in juvenile normal human fibroblasts exposed to simulated microgravity," *Scientific Reports*, vol. 9, no. 1, 2019.

[36] T. J. Corydon, V. Mann, L. Slumstrup et al., "Reduced expression of cytoskeletal and extracellular matrix genes in human adult retinal pigment epithelium cells exposed to simulated microgravity," *Cellular Physiology and Biochemistry*, vol. 40, no. 1–2, pp. 1–17, 2016.

[37] V. Mann, D. Grimm, T. J. Corydon et al., "Changes in human foetal osteoblasts exposed to the random positioning machine and bone construct tissue engineering," *International Journal of Molecular Sciences*, vol. 20, no. 6, p. 1357, 2019.

[38] P. Bradbury, H. Wu, J. U. Choi et al., "Modeling the impact of microgravity at the cellular level: implications for human disease," *Frontiers in Cell and Developmental Biology*, vol. 8, 2020.

[39] A. A. Brinley, C. A. Theriot, M. Nelman-Gonzalez et al., "Characterization of Epstein-Barr virus reactivation in a modeled spaceflight system," *Journal of Cellular Biochemistry*, vol. 114, no. 3, pp. 616–624, 2013.

[40] P. Emma and A. Kamen, "Real-time monitoring of influenza virus production kinetics in HEK293 cell cultures," *Biotechnology Progress*, vol. 29, no. 1, pp. 275–284, 2013.

[41] I. Martínez-Monge, J. Albiol, M. Lecina et al., "Metabolic flux balance analysis during lactate and glucose concomitant consumption in HEK293 cell cultures," *Biotechnology and Bioengineering*, vol. 116, no. 2, pp. 388–404, 2019.